Neuron, Vol. 19, 927–938, October, 1997, Copyright ©1997 by Cell Press

Changes in Permeability Caused by Connexin 32 Mutations Underlie X-Linked Charcot-Marie-Tooth Disease

Seunghoon Oh, Yi Ri, Michael V. L. Bennett, E. Brady Trexler, Vytas K. Verselis, and Thaddeus A. Bargiello*
Department of Neuroscience
Albert Einstein College of Medicine
Bronx, New York 10461

Summary

The relationship between the loss of connexin 32 function and clinical manifestations of X-linked Charcot-Marie-Tooth (CMTX) disease is unknown. Here, we report that eight of nine CMTX mutations investigated form channels with measurable electrical conductance. Single-channel studies of two mutations demonstrate reduced junctional permeability caused by a decrease in either pore size (S26L) or open channel probability (M34T) that favors residency in a low-conductance substate. Permeation of second messengers such as cAMP through reflexive gap junctions between adjacent cytoplasmic loops of myelinating Schwann cells is likely to be reduced or absent in these channels. We propose that CMTX mutations impair the transduction of signals arising from normal glial-neuronal interactions and thereby cause demyelination and axonal degeneration.

Introduction

Charcot-Marie-Tooth disease comprises a common but heterogeneous group of inherited late onset peripheral neuropathies that display similar clinical manifestations characterized by loss of sensation and progressive weakness and by atrophy of distal muscles (Vance, 1991; Suter et al., 1993). It is well-established that loss-of-function mutations of Cx32, a member of the gene family encoding gap junctions, underlie the etiology of the X-linked form of the disease (Bergoffen et al., 1993; Fairweather et al., 1994; Bennett, 1994; Ionasescu et al., 1994, 1995; Orth et al., 1994; Bone et al., 1995). Nearly 90 mutations associated with X-linked Charcot-Marie-Tooth disease (CMTX) have been mapped to the coding region of Cx32 (Scherer, 1997), including several missense mutations that fail to produce functional channels when exogenously expressed in pairs of Xenopus laevis oocytes (Bruzzone et al., 1994a; Omori et al., 1996). The clinical manifestations of the disease vary considerably among affected individuals. In general, heterozygous females are less severely affected than hemizygous males carrying CMTX mutations. This incomplete dominance presumably arises as a consequence of X chromosome inactivation in heterozygous females that would lead to a mosaic of wild type and mutant myelin. The ability of some CMTX mutations to behave as dominant negative suppressors of Cx32 in exogenous expression systems (Omori et al., 1996) cannot explain the observed phenotypic effects of CMTX mutations, since only one X chromosome is active in somatic cells. The phenotype could arise if CMTX mutations behaved epistatically by suppressing the function of other connexins that may be normally coexpressed in Schwann cells, but the expression of other connexins subject to trans-dominant effects has not yet been demonstrated in myelinating Schwann cells. A recent study of 27 CMTX families has suggested that nonsense mutations of Cx32 may produce more severe forms of the disease than missense mutations (Ionasescu et al., 1996). However, as missense mutations can result in functional channels with altered properties as well as nonfunctional channels, biophysical characterizations of channels formed by missense mutations are required to determine the molecular basis of the loss of Cx32 function and to establish if changes in function correlate with the severity of the disease.

In peripheral nerve, Cx32 is found in myelinating Schwann cells, where it is believed to form reflexive gap junctions (Scherer et al., 1995) that shorten the communication pathway between the periaxonal cytoplasm and the peripheral cytoplasm in which the cell nucleus is located. It is likely that reduced communication through this pathway perturbs some aspect of normal glial-neuronal interactions that are critical to the maintenance of myelin sheaths and axons (Doyle and Colman, 1993). The characterization of CMTX mutations that only partially alter channel function should help to establish the critical features of this signaling pathway and the etiology of CMTX disease.

Results

Genetic Analysis of the N Family

The N family, whose pedigree is shown in Figure 1A, has been extensively examined for symptoms of CMT disease (Ohnishi et al., 1995). The proband III-1 is a 28-year-old male presenting moderate manifestations of the disease, including reduction in nerve conduction velocity and extensive demyelination and atrophy of the sural nerve. The coding region of Cx32 (nt 852) of the proband was amplified by the polymerase chain reaction (PCR) from genomic DNA using oligonucleotide primers corresponding to the published sequence of human Cx32 (Kumar and Gilula, 1986). Sequencing of ten independent clones revealed the same C→T transition at nucleotide 77 (Figure 1B), which results in a nonconservative amino acid substitution, S26L, located in the first transmembrane domain of Cx32. With the exception of Cx33, which contains a Lys residue at this position and does not form functional channels in Xenopus oocytes (Bruzzone et al., 1994b; Chang et al., 1996), Ser or Thr residues are conserved among the remaining 12 members of the connexin gene family at this position. The coding region of Cx32 from individuals I-2, II-3, and II-4 was amplified by PCR, cloned, and sequenced. Of seven independently isolated clones from female I-2, four contained the S26L mutation and three were wild type, indicating that the maternal grandmother was heterozygous

* To whom correspondence should be addressed.

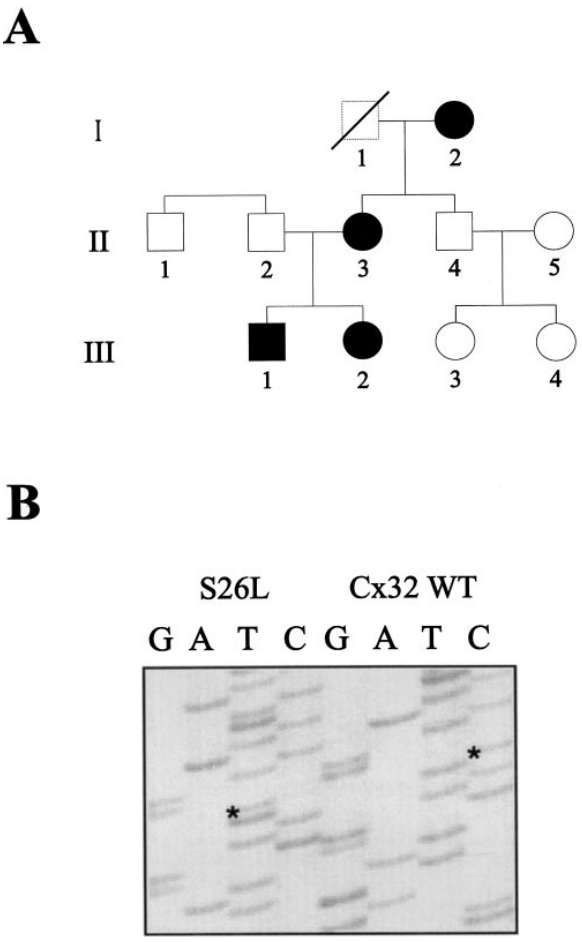

Figure 1. Genetic Analysis of N Family

(A) The pedigree of the N family. Individuals displaying symptoms of CMT disease are indicated by the closed symbols. The proband's (individual III-1) maternal grandfather, I-1, is deceased.

(B) DNA sequence of Cx32 from the proband and an unrelated wild-type individual is shown. The asterisks mark the C→T transition that results in a missense mutation.

for the mutation. Similarly, six wild type and six mutant clones were obtained from the proband's mother, individual II-3 in the pedigree. The unaffected male II-4 had only wild-type Cx32 (12 clones sequenced). The correlation of this mutation with the genetic pedigree indicates that the S26L mutation is the likely cause of CMT in the N family.

The S26L Mutation and Other CMTX Mutations Form Functional Channels

In contrast to several other CMTX mutations, but like CMTX mutations that truncate the carboxyl terminus of Cx32 (Rabadan-Diehl et al., 1994; Omori et al., 1996), the S26L mutation forms functional channels when expressed in pairs of Xenopus oocytes. The junctional conductance-transjunctional voltage (G_j-V_j) relations (where G_j is the junctional conductance, g_j, normalized to the value at $V_j = 0$) and the time course of current relaxations are similar in the S26L mutant and human wild type. Both display a substantial residual conductance (normalized, G_{min}) of 25%–30% at large voltages in the steady-state G_j-V_j relation and a calculated gating charge of ~2. The voltage at which conductance is half maximal, $V_{1/2}$, is shifted by ~15 mV toward zero in the mutant junction from the 45–50 mV of the wild-type junction (Figures 2A and 2B). This shift corresponds to a difference in free energy of ~350 cal/mole between the open and closed states. The similarity of the voltage dependence suggests that the S26L substitution did not alter substantially the structure of the channel.

Given the ability of S26L to form functional channels, we examined four other CMTX mutations (I30N, M34T, V35M, and V38M) that lie within the first transmembrane domain of Cx32. As illustrated in Figures 2C–2H, these mutations form functional channels when expressed either homotypically or heterotypically with Cx32 in pairs of Xenopus oocytes. Of this set of mutations, the effect of the I30N substitution appears to be the least severe. The conductance-voltage relation of the homotypic I30N junction resembles that of S26L, in that it displays a small shift in $V_{1/2}$ to ~30 mV and does not alter the calculated gating charge (Figure 2C). In contrast, the conductance-voltage relations of M34T, V35M, and V38M differ from wild type and suggest that structural and functional perturbations have occurred. The conductance-voltage relation of V35M is most altered. In homotypic pairings, junctional currents are substantially reduced to levels barely detectable (data not shown). In heterotypic V35M/Cx32 junctions (Figure 2H), the conductance-voltage relation is shifted such that junctional conductance is maximal at −75 mV and reduced by ~20-fold at zero transjunctional voltage. The conductance-voltage relation of this heterotypic junction can be explained by a large shift in the conductance-voltage relation of the mutant hemichannel (see Harris et al., 1981; Verselis et al., 1994; Figure 2 legend) that reduces the open probability of the hemichannel at $V_j = 0$. The low open probability of the mutant hemichannel at $V_j = 0$ is consistent with the barely detectable junctional conductance observed in homotypic V35M junctions and suggests that the low conductance is not due to failure of the mutant junctional protein to form hemichannels that reach the membrane surface.

In heterotypic pairings with Cx32, both M34T and V38M display qualitatively similar behavior to V35M, in that they produce considerable shifts in their G_j-V_j relations (Figures 2F and 2G). In both cases, maximal junctional conductance is ~5× greater than the conductance at $V_j = 0$, suggesting that open probability of these two hemichannels has been reduced at this voltage. Both M34T and V38M homotypic junctions express junctional currents. The G_j-V_j relation of homotypic M34T junctions (Figure 2D) is altered more than that of V38M (Figure 2E), suggesting that the open probability of the V38M hemichannel at $V_j = 0$ would be greater than that of M34T in homotypic pairings.

In addition, we examined the expression of four other CMTX missense mutations (G12S, P87A, E102G, and Δ111–116) that lie outside of TM1. Of these, only G12S failed to express junctional currents in homotypic pairings and in heterotypic pairings with Cx32. G12 is believed to initiate the formation of a reverse turn that positions the amino terminus of Cx32 into the channel

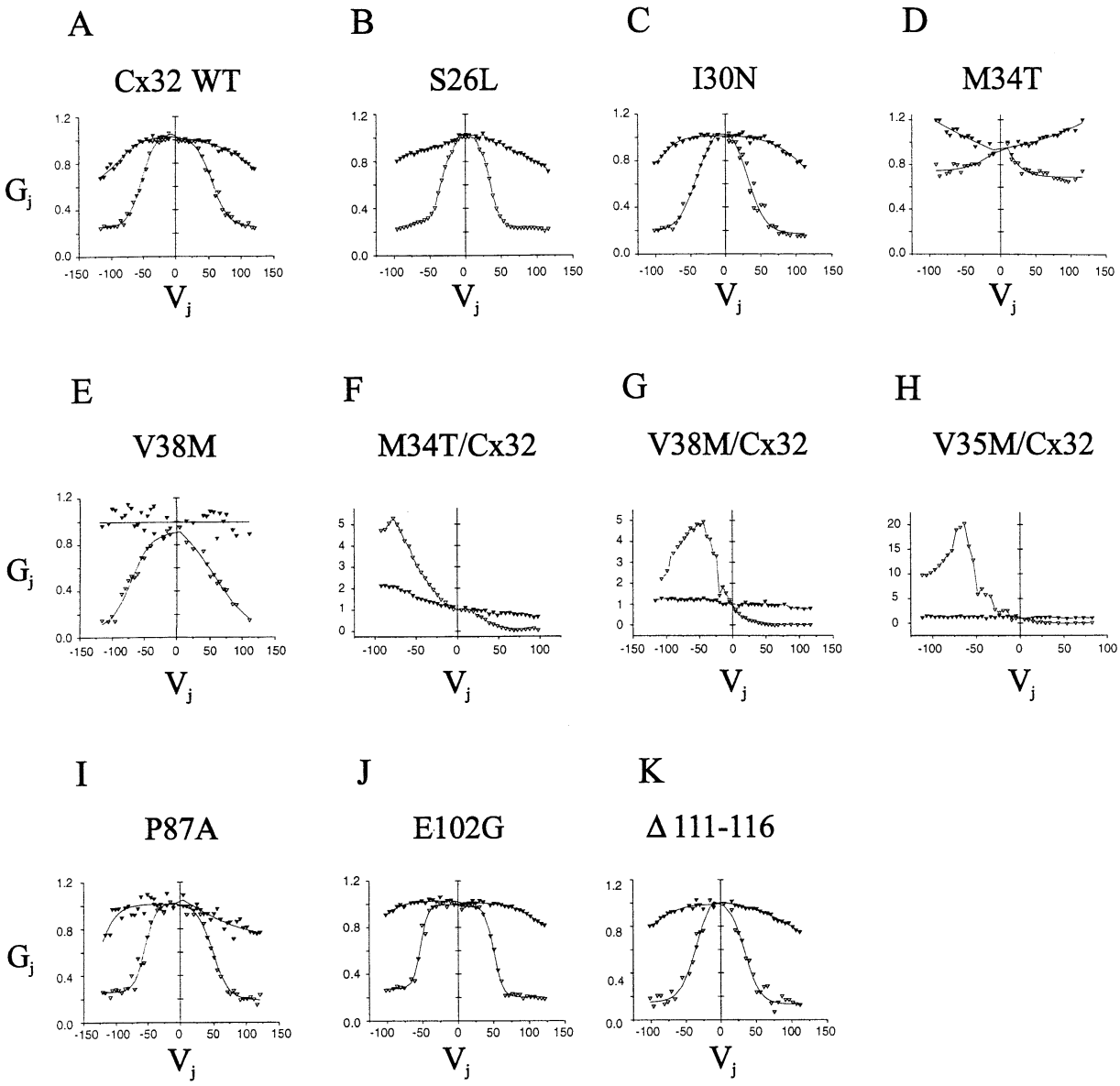

Figure 2. Conductance-Voltage Relations of Junctions Formed by Wild-Type Human Cx32 and Eight CMTX Mutations

Data were obtained from macroscopic recordings of pairs of Xenopus oocytes following injection of in vitro synthesized RNA. Conductances are normalized to the value predicted at $V_j = 0$. Closed triangles denote initial conductances; open triangles denote steady-state conductances. When possible, the data were fit to a Boltzmann relation of the form described by Rubin et al. (1992). In the heterotypic pairings illustrated in (F)–(H), the transjunctional voltage plotted corresponds to voltage applied to the cell expressing Cx32. As the Cx32 hemichannel closes on the application of transjunctional potentials relatively negative at its cytoplasmic face, the decreased conductance observed at relatively positive potentials in the heterotypic records reflects the closure of the mutant hemichannel.

pore (see Verselis et al., 1994). It is possible that the G12S substitution prevents the formation of this turn, or, alternatively, it may disrupt the normal cellular processing of Cx32. The remaining three mutations, P87A, E102G, and Δ111–116, all form functional junctions whose macroscopic properties do not differ substantially from wild-type Cx32 when expressed in pairs of Xenopus oocytes (Figures 2I–2K). E102G and Δ111–116 are located in the cytoplasmic loop of Cx32, a domain that interacts with the amino terminus and may influence pore structure (S. O. et al., unpublished data). Similarly, the P87A substitution may alter transmembrane helix interactions by changing the degree of twist caused by a proline kink motif present in wild-type TM2 and consequently may change the conformation of amino acids that line the pore (Barlow and Thornton, 1988; Ballesteros and Weinstein, 1992; Sankararamakrishnan and Vishveshwara, 1992; Suchyna et al., 1993; Y. R. et al., unpublished data).

The observation that five mutations (S26L, I30N, P87A, E102G, and Δ111–116) form functional gap junctions whose voltage dependence does not differ substantially from wild type, yet cause the CMTX disease phenotype, suggests that alterations in junctional permeability are

responsible for the loss of Cx32 function underlying CMTX. The macroscopic behaviors of the other three mutants (M34T, V35M, and V38M), in which open probability appears to be substantially reduced, are consistent with this hypothesis. To investigate further the permeability of junctions formed by CMTX mutations, we examined the single-channel properties of two mutations located in TM1: S26L, which displays a nearly wild type conductance-voltage relation, and M34T, which displays a substantial shift in its conductance-voltage relation. The coding regions of human wild-type Cx32, S26L, and M34T were transfected into the mouse Neuro-2A (N2A) cell line. Two stably transfected human Cx32 wild type, two S26L, and three M34T cell lines were characterized. Expression of transfected connexin genes in each cell line was confirmed either by immunocytochemistry using a monoclonal antibody provided by Dr. E. Hertzberg that recognizes an epitope in the cytoplasmic loop of Cx32 or by DNA sequencing of RT-PCR products of mRNA isolated from each transfected cell line (data not shown). There was no evidence of endogenous connexin expression in the cell lines used in this study.

Comparisons of Unitary Conductances of Wild Type and S26L Gap Junctions

Single-channel records of Cx32 gap junctions formed by wild type and the S26L mutation are presented in Figure 3. The S26L mutation has little if any effect on the unitary conductance of wild-type Cx32 channels, when records are obtained with internal pipette solutions containing 140 mM CsCl. In both cases, the application of transjunctional voltage (V_j) elicits a current corresponding to a junctional conductance of ~70 pS (see position 1 in Figures 3A and 3B; and all-points histograms in Figures 3D and 3E). We ascribe this conductance to the fully open channel. Subsequently, transitions of ~45 pS, ~50 pS, and ~60 pS are evident in both records. Although the low frequency of gating events observed in these records complicates analysis of the relation among these transitions, they are suggestive of the presence of discrete subconductance states. The lack of any superimposition of open states is consistent with the presence of a single-channel with transitions between a 70 pS main open state and three subconductance states of ~25, 20, and 10 pS (see Figures 3C and 3F). In addition to these transitions, both mutant and wild-type channels can display complex gating transitions that are not resolvable as discrete events and result in complete channel closure (position 2 and 2′ in Figures 3A and 3B). They are similar in appearance to the docking currents associated with channel formation and with complete closure (Bukauskas and Weingart, 1994); they also resemble loop gating in Cx46 hemichannels (Trexler et al., 1996). They most likely represent a different gating mechanism than the fast and discrete transitions ascribed to V_j-dependence.

The probability that the wild type and mutant channels reside in the fully open state, determined from the ratio of areas under the peaks in the all points histograms corresponding to these records (Figures 3D and 3E), is 0.4 and 0.3, respectively. At smaller transjunctional voltages (10 and 20 mV), both wild type and mutant channels reside almost exclusively in the fully open state (data not shown). Thus, as suggested by the similarities in the conductance-voltage relations (Figure 2B), the mutation does not appear to change markedly the open probability of the channel at all transjunctional voltages examined. As there is unlikely to be any transjunctional voltage gradient across reflexive gap junctions present within Schwann cells, we expect that both wild type and mutant channels will be fully open under normal physiological conditions.

A difference in the conductance of wild type and S26L channels was observed when the internal pipette solutions contained 145 mM LiCl (Figure 4). The conductance of the fully open channel and average size of the gating transitions were 54 ± 5.9 and 40 ± 1.8 pS, respectively, for the wild-type channel (three cell pairs) and 43 ± 2.9 and 30 ± 2.7 pS for the S26L mutation (six cell pairs). The difference in the size of the gating transitions is statistically significant ($t = 6.20$; $p < 0.001$).

Determination of the Pore Size of Wild Type and S26L Channels

To examine if the reduction in conductance of the S26L mutation in LiCl recording solutions resulted from a decrease in the channel radius, we determined how current flow through the wild type and S26L mutant channels was affected by a series of nonelectrolytes with differing hydrodynamic radii and viscosities (Vodyanoy and Bezrukov, 1992; Bezrukov and Vodyanoy, 1993; Krasilnikov et al., 1995). The presence of a nonelectrolyte in the channel pore is expected to cause a significant reduction in single-channel conductance as a consequence of several possible factors, including block, reduction in dissolved salt activity, and an increase in the bulk solution resistivity. Exclusion of the nonelectrolyte from the aqueous pore should affect only the access resistance of the channel, which, in the case of the single-channel measurements of gap junctions, is expected to make only a small contribution to total channel resistance. In wild-type channels, a large change in unitary conductance occurs when polyethylene glycol (PEG) 300 or smaller molecules are included in the recording solution (Figure 5). The simplest interpretation of this result is that molecules with a hydrodynamic radius ≤5.8 Å can occupy the pore and that the effective pore radius of the wild-type channel is between 6 and 7 Å. In contrast, the conductance of the S26L channel remained constant at the maximum level for all nonelectrolytes tested and was similar to the conductance of the wild-type Cx32 channels for PEGs that could not enter the wild-type channel pore. Thus, the radius of the mutant channel pore is smaller than the hydrodynamic radius of glycerol, ~3.1 Å, the smallest nonelectrolyte tested.

Ionic Permeabilities of Wild Type and S26L Channels

We further examined permeability through the S26L mutant channel by using ionic gradients and biionic conditions. In a 10:1 CsCl gradient osmotically balanced with mannitol, the reversal potential (E_{rev}) of the S26L channel is 5.6 mV (Figure 6A), indicating slight anion selectivity.

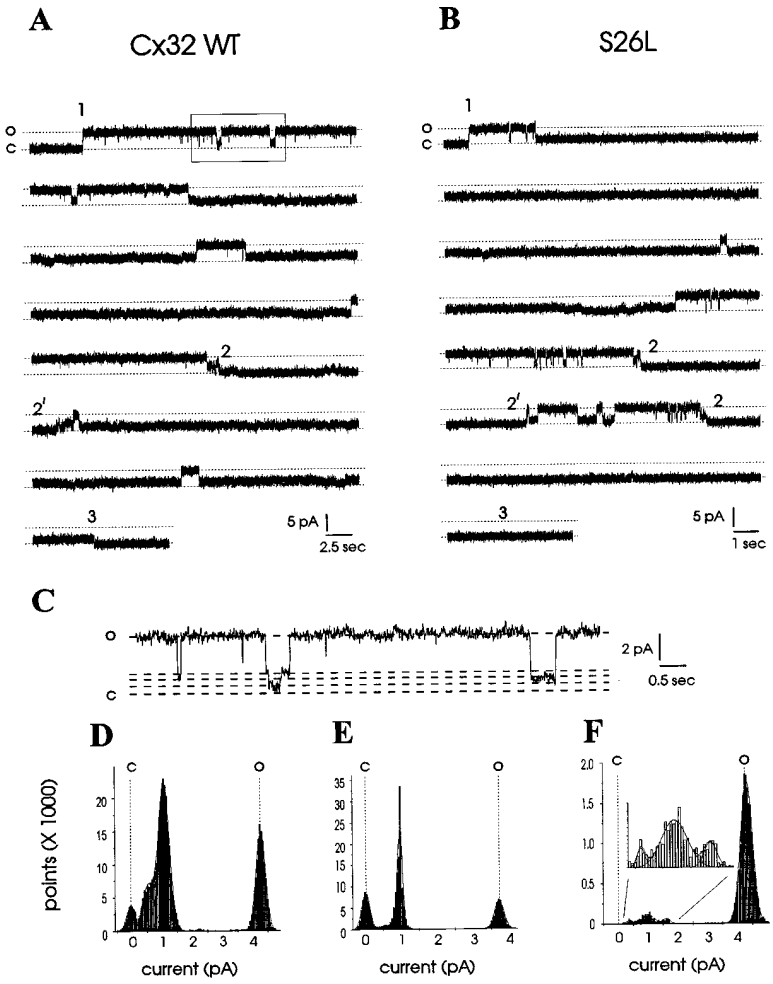

Figure 3. Continuous Single-Channel Records of Wild-Type Human Cx32 (A) and S26L (B), Respectively, Obtained from Pairs of Transfected Neuro-2A Cells in Double Whole-Cell Patch Recording with 140 mM CsCl Pipette Solutions

Initially, both cells were voltage clamped at 0 mV. Transjunctional voltages (V_j) were applied by stepping one cell over a range of −80 to +80 mV. The current traces recorded from the unstepped cell shown in (A) and (B) correspond to junctional currents, I_j, elicited by V_j steps of −60 mV and −55 mV, respectively. Changes in junctional current are reflected by equal and opposite transitions in the current trace of the stepped cell (data not shown). The dashed lines indicate the fully open (o) and fully closed states (c). The numbers 1 and 3 mark the onset and termination of the V_j step, the number 2 marks a slow gating event to the fully closed state, and 2′ a slow gating event to the fully open state. In the wild-type record shown, an ~20 pS step was observed at the termination of the V_j step (position 3), indicating that the channel was in the 20 pS subconductance state at this time. The magnitude of the subconductance state accounts for the 30% G_{min} observed in macroscopic recordings. No change in conductance was observed in this record of the S26L channel at the end of the V_j step because the channel had entered the fully closed (nonconducting) state by a slow gating transition prior to the termination of the V_j step. (C) The boxed region of the wild-type record is expanded. The dashed lines indicate the fully open (o), fully closed (c), and three subconductance states. (D–F) All points histograms corresponding to traces (A), (B), and (C), respectively. The dashed lines indicate the current levels of open and closed states depicted in the single-channel traces. In (F), the region of the histogram between 0 and 2 pA is magnified to show the resolution of three possible channel substates. Data were filtered at 1 kHz with a four-pole low pass Bessel filter and digitized at 5 kHz using an Axopatch 200B integrating patch amplifier and a Digidata 1200A interface (Axon Instruments, Foster City, CA). The portion of the record shown in (C) was digitally filtered at 50 Hz for presentation. All points histograms were constructed with a bin size of 0.05 pA and fit to a Gaussian using Origin 4.0 software (Microcal Software Inc.).

The relative permeability of Cl^- to Cs^+ (P_{Cl}/P_{Cs}) is 1.3 using the Goldman-Hodgkin-Katz (GHK) voltage equation. A similar result was obtained for the wild-type channel (E_{rev} = 7.6 ± 3.2 mV; data not shown), although the permeability of mannitol in wild-type channels (see Figure 5) may have caused the reversal potential to be shifted slightly toward zero. Similar anion selectivity of Cx32 channels has been reported (Harris et al., 1992; Veenstra, 1996). Using biionic conditions and the GHK voltage equation with E_{rev} = 11.8 mV (Figure 6B) and assuming P_{Cl}/P_{Cs} = 1.3 (see Experimental Procedures), we determined that P_{Li}/P_{Cs} in the mutant channel was ~0.15. This value for P_{Li}/P_{Cs} is substantially less than that predicted by the diffusion coefficients of Li^+ and Cs^+ in bulk solution where P_{Li}/P_{Cs} = 0.5, indicating a substantial decrease in permeability of the mutant channel to Li^+. Based on the observed conductance in CsCl solutions, the permeability ratios calculated for Cs^+, Li^+, and Cl^- predict a conductance of 44 pS for the fully open mutant channel in symmetric 145 mM LiCl. This value is in close agreement with that observed (43 ± 2.9 pS). Similarly, the conductance of the fully open wild-type channel in LiCl can be predicted from the conductance observed in CsCl solutions and the Cl/Cs permeability ratio (54 ± 5.9 pS observed versus 55 pS predicted), if one assumes that Cs^+ and Li^+ permeate the wild-type channel according to their bulk solution mobilities. The simplest explanation for these results is that ions permeate gap junctions formed by wild-type Cx32 and S26L by free diffusion. The reduction in unitary conductance of the mutant channel observed in LiCl (~40%) is likely to arise as a consequence of its smaller pore radius, less than 3.1 Å, which is close to that of a hydrated Li^+ ion, ~3 Å (Hille, 1975).

Single-Channel Behavior of M34T Channels in Transfected N2A Cells

Figure 7A illustrates that the single-channel behavior of the M34T substitution is substantially different from wild type. The application of a transjunctional voltage step of −80 mV (at position 1 in trace [a]) elicits a junctional current, resulting in a 15 pS conductance as determined

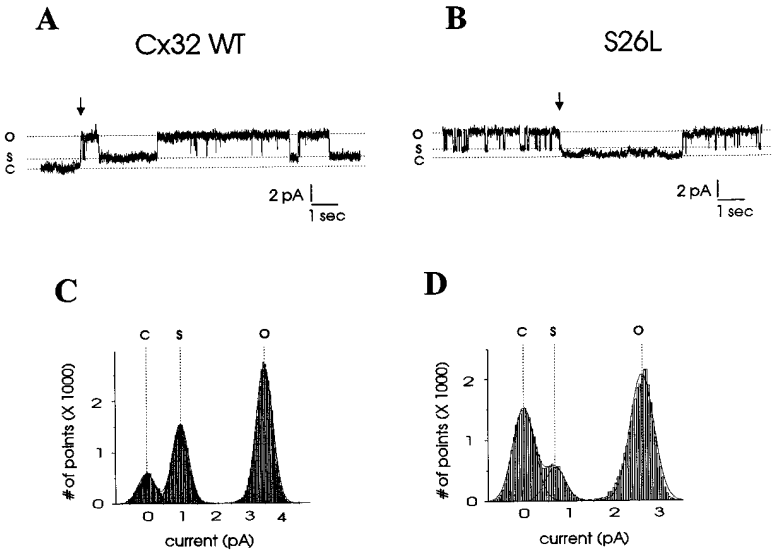

Figure 4. Segments of Double Whole-Cell Patch Records Representative of Wild-Type Human Cx32 and the S26L Mutation Obtained with Pipette Solutions Containing 145 mM LiCl

(A) In the record from a wild-type channel, a transjunctional voltage of −60 mV was applied at the arrow. Conductance of the fully open state, determined by the all points histogram shown in (C), was 58 pS; the conductance of the substate was 16 pS.

(B) In the segment of the S26L record (recorded at $V_j = -60$ mV), two different transitions (31 and 43 pS) are evident, as determined by the all points histogram shown in (D). The large transition (43 pS) indicated by the arrow corresponds to a complex gating transition (loop gating) and reflects the conductance of the fully open channel. The smaller transition is between the fully open state and a substate. In two cell pairs expressing a single S26L channel, the conductance of the fully open channel at the application of a V_j step was ~45 pS (data not shown).

(C and D) All points histograms corresponding to traces (A) and (B), respectively. The dashed lines indicate the current levels of open, sub-, and closed states depicted in the single-channel traces shown in (A) and (B).

Data were filtered at 1 kHz with a four-pole low pass Bessel filter and digitized at 5 kHz using an Axopatch 200B integrating patch amplifier and a Digidata 1200A interface (Axon Instruments, Foster City, CA). In (A) and (B), records were subsequently digitally filtered at 250 Hz for presentation. All points histograms were constructed with a bin size of 0.05 pA and fit to a Gaussian using Origin 4.0 software (Microcal Software Inc.). Pipette resistances were 5–10 MΩ.

by the all points histogram shown in Figure 7B. The channel makes brief transitions to an ~65 pS state (48 pS transition at position 2 in trace [c]) that does not differ substantially from the ~70 pS conductance of the fully open Cx32 wild-type channel. We believe that the 15 pS conductance corresponds to a channel substate. As illustrated by the all points histogram (Figure 7C), the M34T channel resides in this low-conductance substate ~98% of the time at −80 mV. Furthermore, the application of any magnitude of transjunctional voltage step from $V_j = 0$ almost invariably results in a 15–20 pS conductance, indicating that the channel resides predominantly in a low-conductance substate at $V_j = 0$. Thus, it appears that the major effect of the M34T mutation is to cause a large reduction in open channel probability without causing substantial changes in the conductance of the fully open channel. These data are consistent with the macroscopic behavior of the channel shown in Figures 2D and 2F. We have not directly examined permeation through the fully open or substates of M34T channels, but a large decrease in junctional permeability would be caused by the reduction in open time, which favors channel residence in a low permeability substate.

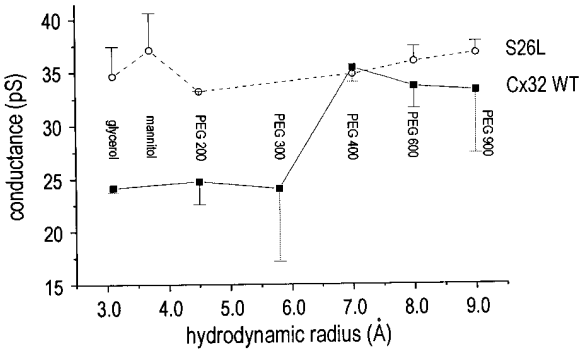

Figure 5. The Effect of Nonelectrolytes on the Conductances of Wild Type and S26L Channels

The conductance, determined by all points histograms, of wild-type Cx32 channels (closed squares) and S26L mutant channels (open circles) is plotted as a function of the hydrodynamic radius of a series of nonelectrolytes that were included in the recording solution. For S26L channels, the conductance is essentially unaffected by the nonelectrolytes used and is near the maximum observed for wild-type channels. In the case of wild-type channels, the conductance rises sharply between PEG 300 and PEG 400. The large standard deviation of the mean for PEG 300 in the wild-type channel results from a bimodality in the conductances observed. In four cell pairs, the mean conductance was 20 ± 1.8 pS, indicating that PEG 300 had entered the channel, whereas in two cell pairs, the mean conductance was 33 ± 2.0 pS, indicating that PEG 300 was excluded. The bimodality of the data suggests that the wild-type channel may occupy other long-lived states that we have not distinguished in our single-channel recordings or may be assembled in different conformations with altered permeability but not conductance. Molecules larger than PEG 300 were always excluded.

Discussion

Structural Implications of the S26L and Other TM1 Mutations

The similarity of single-channel conductance of mutant and wild-type channels in CsCl solutions and exclusion of nonelectrolytes larger than glycerol can be explained if the S26L mutation forms a constriction near the mouth of the channel (Figure 8A). In this model, the access resistance at either end of the mutant channel in CsCl would not differ substantially from that of wild type. Consequently, the flux of ions that pass through either channel would be determined predominantly by the resistance associated with the entire length of the pore.

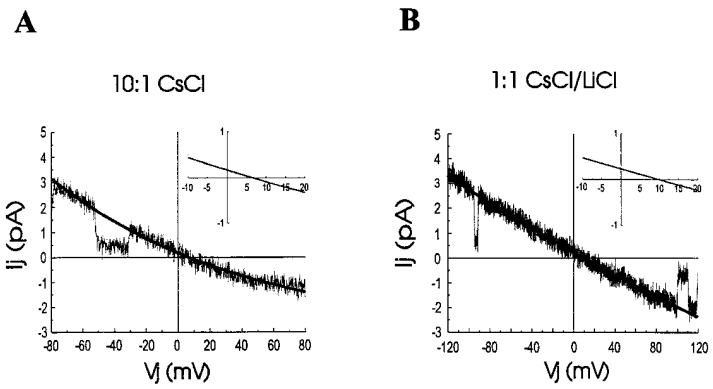

Figure 6. Reversal Potentials of S26L Channels in Salt Gradients and Biionic Conditions

Ramp voltages between −80 and +80 mV were applied to one cell.

(A) A representative determination of the reversal potential (E_{rev}) of a single S26L channel in a 10:1 CsCl gradient. The junctional current trace was fit to a single exponential function and is representative of 60 consecutive 1.24 s voltage ramps applied to the cell containing the higher salt concentration. The insert shows a portion of the fit of the junctional currents, indicating E_{rev} = 6.5 mV. The average E_{rev} was 5.6 ± 1.8 mV for the 60 traces, which corresponds to a permeability ratio P_{Cl}/P_{Cs} = 1.3 using the Goldman-Hodgkin-Katz (GHK) voltage equation.

(B) A representative trace and E_{rev} of a single S26L channel under biionic conditions (1:1 LiCl/CsCl). The reversal potential was 9.5 mV (see insert); the average E_{rev} determined from 120 ramps applied to the cell containing LiCl was 11.8 ± 1.1 mV, corresponding to a P_{Li}/P_{Cs} of 0.15, calculated by the GHK voltage equation assuming P_{Cl}/P_{Cs} = 1.3 (see Experimental Procedures).

In the case of ions with a small hydrated radius, such as Cs^+ (1.8 Å radius; Hille, 1975), the region where the serine residue is located would make only a small contribution to the total channel resistance, and this would not be changed significantly by the leucine substitution (see Figure 8A legend). However, the reduction in pore size caused by the presence of leucine residues near the mouth of the mutant channel would have a larger effect on the passage of molecules whose size approaches that of the channel opening, ~3 Å (see Renkin, 1954; Solomon, 1986), explaining both the observed exclusion of nonelectrolytes and the decreased permeability to ions with a larger hydrated radius. These considerations suggest that the first transmembrane domain of Cx32 contributes to the lining of the aqueous pore of the gap junction channel. This conformation contrasts with existing models of gap junction topology inferred entirely from amino acid sequence but is consistent with the observation that charged amino acid residues located at the border of the first transmembrane domain and first extracellular loop (TM1/E1) contribute to the formation of the Cx32 transjunctional voltage sensor (Verselis et al., 1994) and therefore should lie close to the aqueous pore.

Recently, Zhou et al. (1997) investigated the accessibility to the thiol reagent maleimido-butyryl-biocytin of cysteine substitutions of amino acid residues in a conducting hemichannel formed by the Cx32 chimera, Cx32*Cx43E1. They concluded that TM1 contributes to the lining of this channel. Contrary to the prediction from our data, the S26C residue was not modified by their reagent. This result may have been a consequence of two factors: extracellular application of the reagent, which would be quite distant from the S26C residue, and steric hindrance, as the thiol reagent used is large (537 Da), with molecular dimensions somewhat larger than the radius we predict for the Cx32 pore. We cannot at this time exclude the alternative possibility that the leucine substitution at S26 resides deeper in the wall of the channel and causes a conformational change that pushes a pore lining residue inward to obstruct the lumen. However, we feel that this hypothesis is less likely, as the mutation would be expected to change the structure of the channel substantially, whereas the similarity of the voltage dependence of S26L and wild-type channels suggests that significant structural perturbations do not occur. We are currently investigating the accessibility of S26C in Cx32 junctions to smaller thiol reagents.

Recently, Unger et al. (1997) reported the structure of Cx43 gap junctions channels at 7 Å resolution. Their work indicates that gap junctions comprise four membrane-spanning domains that adopt an α-helical conformation. Figure 8B shows the position of the five CMTX missense mutations investigated in this study on the axial projection of an α-helical representation of the backbone of TM1. The magnitude of the shift in the conductance-voltage relations of the five missense CMTX mutations that lie within TM1 is correlated with their position in this representation. S26L and I30N mutations, which produce the smallest changes in their conductance-voltage relations, are flanked by residues M34 and I33, which have been shown to be accessible to cysteine modification reagents (Zhou et al., 1997). Therefore, all four residues, I30, S26, I33, and M34, may lie in the permeation pathway of the open channel. The mutation demonstrating the largest change in macroscopic behavior, V35M, is furthest from the helical face formed by I33 and M34, raising the possibility that it has significant interactions with other transmembrane helices. Such interactions could explain the large shift observed in the G_j-V_j relation of this mutation. The similarity of the single-channel conductance of the open state of M34T to wild type is reasonable, as the bulk of the threonine side chain is somewhat smaller than that of the methionine residue present in the wild-type channel.

Implications for CMTX

In this paper, we report that eight of nine missense CMTX mutations that we have examined form functional channels. Three mutations, M34T, V35M, and V38M, cause substantial shifts in the conductance-voltage relation that would likely cause significant reductions (5- to 20-fold) in channel open probability. Single-channel studies of M34T support this interpretation and demonstrate that under normal physiological conditions, the channel would reside predominantly in a 15–20 pS substate. It is interesting to note that the same mutation,

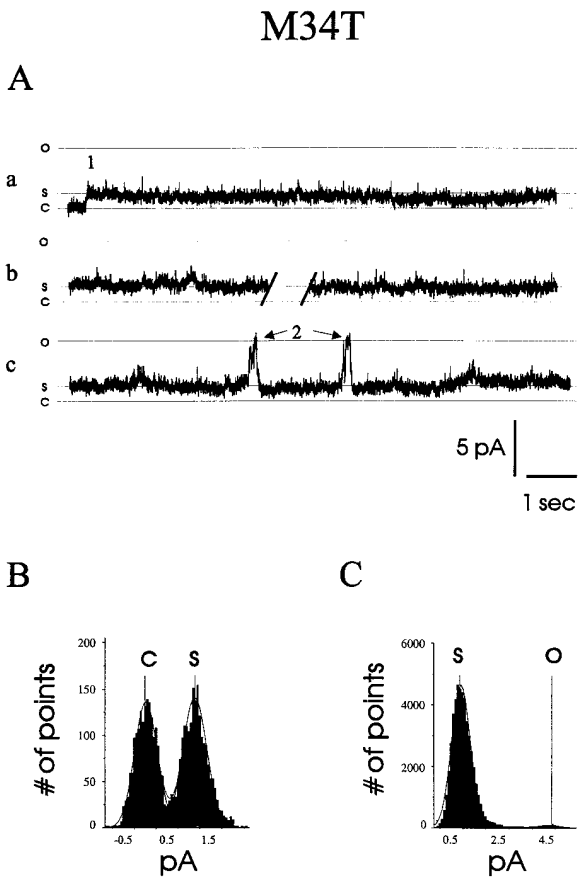

Figure 7. Representative Segments of an ~3 Min Single-Channel Record of M34T

At position 1 in trace (a), a transjunctional voltage step of −80 mV was applied that resulted in a current corresponding to a 15 pS junctional conductance. The break in the current record in trace (b) corresponds to approximately 1 min. Position 2 in trace (c) marks two 48 pS transitions from the substate, which result in a 63 pS state that most likely reflects the conductance of the fully open M34T channel. The all points histogram shown in (B) corresponds to the initial second of the record around position 1. The histogram in (C) corresponds to the entire trace (c) in (A). The open probability of the 63 pS state, determined by the area under the peaks, was ~0.02 for this segment of the record, which approximates the behavior of the channel for the entire duration of the record. This result is representative of all M34T single-channel records obtained in three independent stably transfected Neuro-2A cell lines. Records were obtained with 140 mM CsCl pipette solutions. Data were filtered at 1 kHz with a four-pole low pass Bessel filter and digitized at 5 kHz using an Axopatch 200B integrating patch amplifier and a Digidata 1200A interface (Axon Instruments, Foster City, CA). The traces shown were digitally filtered at 250 Hz for presentation. All points histograms were constructed with a bin size of 0.05 pA (B) and 0.1 pA (C) and fit to Gaussians using Origin 4.0 software (Microcal Software Inc.). Pipette resistances were 5–10 MΩ.

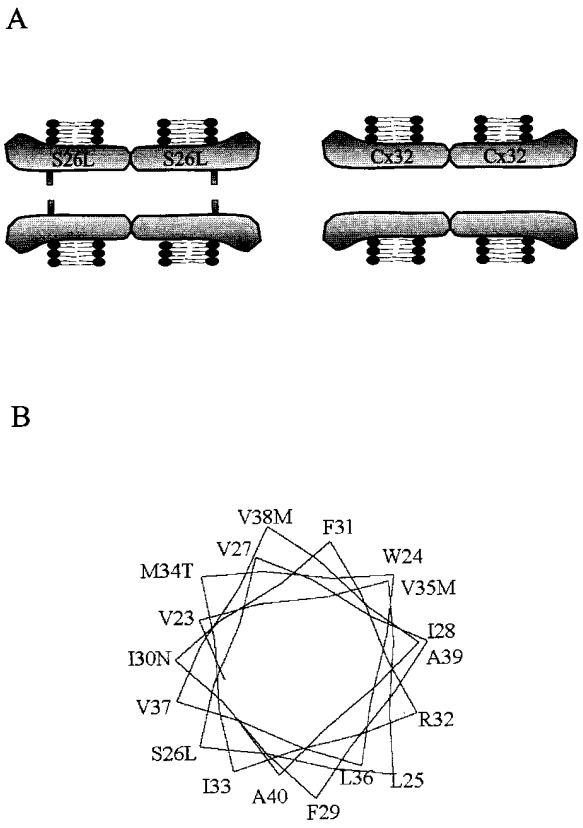

Figure 8. Diagrammatic Representations of S26L and Other CMTX Mutations in TM1

(A) A proposed structural model of a S26L gap junction channel compared to a wild-type Cx32 gap junction channel showing a constriction in the channel pore resulting from the Leu substitution. If the resistance of the wild-type channel, R_{WT}, can be approximated by that of a cylinder of length l and radius r and the resistance of the mutant channel, R_{MUT}, by that of cylinders in series, one of length $(l - 2\Delta l)$ and radius r and two of length Δl and radius r/n, then the ratio of mutant to wild-type resistances is given by $R_{MUT}/R_{WT} = [1 + 2(n^2 - 1)\Delta l]/l$. If R_{MUT} is no more than 10% greater than R_{WT} and n = 2, then $\Delta l/l < 0.02$. Thus, if the leucine residue occupies 2% of the length of the channel pore, the single-channel conductance in CsCl would be changed by only 10%. This narrow a constriction would appear to be a reasonable contribution for a single amino acid to total channel length.

(B) The positions of amino acid residues 23–39 of the first transmembrane domain of Cx32 in the axial projection of an α-helical backbone.

M34T, in Cx26 underlies a form of hereditary nonsyndromic sensorineural deafness (Kelsell et al., 1997).

The S26L mutation reduces channel permeability by causing a substantial reduction in pore radius of the open state. Nonelectrolytes with radii greater than 3.1 Å are excluded from channels formed by the mutation, and permeability to hydrated ions with a radius greater than ~3 Å in radius should be greatly reduced.

The similarity in the electrical conductance of the S26L and wild-type channels in CsCl recording solutions indicates that the loss of electrical coupling in null CMTX mutations is in itself unlikely to cause the disease. Also, the capacity of Schwann cells to buffer local increases in K^+ resulting from neuronal activity will not be affected by the S26L mutation, since K^+ permeability should differ little in mutant and wild-type channels given the similar mobilities of Cs^+ and K^+ in bulk solution.

Although there is cytoplasmic continuity between abaxonal and adaxonal regions of the Schwann cell, gap junctions between successive turns of the cytoplasmic spirals at the paranodes and Schmidt Lantermann incisures should significantly increase communication of

junction permeable molecules between inner and outer regions, as they could decrease the distance traveled by such molecules by several hundred fold. For example, the center-to-center spacing between paranodal cytoplasmic loops is ~0.1 μm, while the circumferential distance around a 10 μm diameter axon is 10π μm for an ~300-fold difference in distance. This calculation assumes a negligible concentration drop across the junctions between loops. The calculated electrical resistance around a 10 μm diameter fiber of a cytoplasmic loop 0.1 μm in diameter with resistivity of 100 Ω cm would be about 4×10^9 Ω or 250 pS, so that as few as five 50 pS channels would provide a significant shunt. For both the reduction in distance and shunting provided by a fixed number of gap junction channels, the effect is greater for larger diameter fibers.

The loss or attenuation of the gap junctional pathway would alter the distribution of stable molecules generated at one site and utilized at a distant site, increasing the concentration of molecules at the former and decreasing them at the latter. The effect on distribution would be greater for short-lived molecules that could be degraded or sequestered en route. Consequently, CMTX disease in the S26L kindred seems likely to arise from reduced intracellular movement of diffusable, possibly short-lived molecules between 3 and 7 Å in radius.

M34T could cause CMTX disease, not by a reduction in permeability of its fully open state, but rather by the reduction in time spent in that state. Our data indicate that the channel resides predominantly in a 15–20 pS substate at physiological conditions. Although we have not determined the permeability of the M34T 15–20 pS substate, it is likely to be impermeable to molecules greater than 3 Å in radius. The ~4-fold decrease in conductance of the substate would be produced by a 50% reduction in pore radius (from 6–7 Å to 3–3.5 Å, or close to that determined for S26L), if we assume that both the fully open channel and substate are uniform cylindrical structures. Even if the permeability of the substate to larger molecules was unchanged relative to that of the fully open state, the flux of molecules would be decreased by at least 4-fold. The reduction in conductance is large enough that the concentration of molecules required for the maintenance of myelin could be reduced below a critical level. Thus, although the S26L and M34T mutations have very different effects on the structure and function of gap junction channels, both may act by reducing permeation of the same molecules.

The large reduction in junctional currents in V35M suggests that the open probability of these channels is significantly reduced, and that like M34T, most V35M channels would reside in a residual conductance state at small V_j. It is possible that the larger fraction of V38M channels is fully open under physiological conditions, as the G_j-V_j relation of V38M homotypic junctions appears to be shifted less than that of M34T and V35M (Figure 2). If permeation through the fully open state of V38M channels does not differ greatly from wild type (which may be true of M34T), then it is possible that a partial rather than complete reduction in macroscopic junctional conductance without change in permeability underlies some cases of CMTX. As discussed above, a partial reduction in macroscopic junctional conductance could result in a substantial change in the distribution of molecules.

There is considerable evidence that the maintenance of myelin sheaths in peripheral nerve requires the continual expression of genes in Schwann cells that are controlled by signals arising from interactions with the axon and that these signals rely on diffusable second messengers (see Mirsky et al., 1980; Salzer et al., 1980; Lemke and Chao, 1988; Monuki et al., 1989; Lemke, 1990; LeBlanc et al., 1992; Poduslo et al., 1995). The data presented in this paper make it unlikely that second messengers such as IP3, cAMP, cGMP, or Ca^{2+} would permeate either the S26L channel or the substate of the M34T channel. Both cAMP and cGMP permeate wild-type Cx32 channels (Bevans et al., 1997), and it is likely that Ca^{2+} with a hydrated radius of 4 Å permeates the ~7 Å radius wild-type channel (see Saez et al., 1989). We favor the hypothesis that the primary defect that underlies CMTX disease in the S26L and M34T kindreds is the reduced permeability of Cx32 junctions, which attenuates second messenger signals, causing alterations in the expression of genes that are required to maintain the differentiated (myelinating) state of Schwann cells. At present, cAMP is the best candidate messenger. It appears that elevations of cAMP in Schwann cells, which may result from direct axonal–Schwann cell contact, are at least partially involved in the induction of genes necessary for myelination (Mirsky et al., 1980; Salzer et al., 1980; Lemke and Chao, 1988; Monuki et al., 1989; Lemke, 1990; LeBlanc et al., 1992) and in the maintenance of the myelin sheath (Poduslo et al., 1995). These genes include those encoding the major myelin structural proteins, protein zero (P_0), myelin basic protein (MBP), and PMP22. It is interesting to note that mutations of genes encoding P_0 and PMP22 underlie CMT1B and CMT1A, respectively. Attenuation of cAMP signals may lead to demyelination as a result of the down-regulation of myelin structural proteins. It is interesting to note that the Cx32 promoter region contains two cAMP response elements (Miller et al., 1988) that may modulate its expression in Schwann cells. The reductions in cAMP permeability that may occur in mutations such as V38M, which reduce macroscopic junctional conductance, may prevent normal Cx32 expression, further exacerbating the effect of the mutation by reducing the number of gap junctional channels formed between myelin.

It is also likely that Schwann cells produce trophic factors that are required for axonal maintenance and that the release of these molecules may require signals whose intracellular propagation is facilitated by gap junctions. The loss of trophic support accompanying dedifferentiation or loss of Schwann cells could explain the axonal degeneration that characterizes CMTX disease. Large, thickly myelinated axons, which would rely more on the gap junctional pathway to facilitate communication between the periaxonal and the peripheral cytoplasm, would be expected to be more susceptible to the disease. This prediction appears to be born out by histological examination of nerve biopsies from CMTX patients (Rozear et al., 1987; Nicholson and Nash, 1993). Large fibers are reduced in number, and the internodal

distance may be decreased, suggesting that remyelination has occurred.

We cannot rule out the possibility that the primary effect of the S26L and M34T mutations is to cause the disruption of cellular homeostasis arising from changes in the cellular distribution of metabolites. The effect would be greatest if the relevant metabolite was short-lived and synthesized in regions distant from where it was utilized and presumably was in limiting supply. ATP may be a good candidate, as it would likely permeate the wild type but not the mutant channels. Alternatively, a toxic metabolic product could accumulate periaxonally in the absence of functional gap junctions leading to the loss of Schwann cells.

Our results do not explain the mechanism(s) responsible for the delay in onset of CMTX disease or its apparent restriction to longer axons. The changes in junctional permeability described here would not change in an age-dependent manner or with axonal length but would be more deleterious in larger diameter axons. Delayed onset could arise if the maintenance of the myelinated state becomes more dependent upon signaling through the gap junctional pathway with increasing age, if the nature of the signaling molecule changes, if the ability of Schwann cells to remyelinate axons decreases following repeated demyelinations, or if the diameter increases sufficiently. It is possible that a large number of Schwann cells must be lost to compromise trophic support to some critical level that initiates axonal degeneration and that this level is lower in longer axons. Detailed anatomical and neurological characterizations of patients at various stages of CMTX disease as well as molecular studies of normal glial-neuronal interactions may allow distinctions to be made among these possibilities and may provide additional clues leading to the identification of critical molecules whose distribution and functional role are affected by the loss of Cx32 function. Future studies of the permeability of the four mutations, I30N, P87A, E102G, and Δ111–116, reported here as well as other CMTX mutations that form channels with wild-type macroscopic properties should be useful in this regard. The molecular mechanisms underlying Schwann cell differentiation and glial-neuronal interactions are being rapidly elucidated (Mirsky and Jessen, 1996; Zorick and Lemke, 1996). These studies may lead to the identification of pharmacological agents including cytokines and trophic factors that maintain the differentiated state of Schwann cells and may provide an effective means of controlling the onset and progression of CMTX disease.

Experimental Procedures

Cell Transfections

The coding regions of wild-type Cx32, S26L, and M34T mutations were cloned in either pXT1 (HSV-TK promoter) or pCI-neo (CMV promoter) and transfected into a mouse Neuro-2A cell line using lipofectin (GIBCO BRL) according to the manufacturer's protocol. Transfected cells were selected with 300 μg/ml (active) G418 (GIBCO BRL).

Electrophysiological Recording

Macroscopic recordings and analysis of junctional currents from pairs of Xenopus oocytes were as described (Rubin et al., 1992). Recording and bath solutions in double whole-cell patch experiments of transfected Neuro-2A cell lines were as follows: in the CsCl experiments, pipette solutions contained 140 mM CsCl, 10 mM TEACl, 2 mM BAPTA, 1 mM $CaCl_2$, 10 mM HEPES (pH 7.2). The cells were bathed in a solution containing 142 mM NaCl, 1.3 mM KCl, 0.8 mM $MgCl_2$, 0.9 mM NaH_2PO_4, 1.8 $CaCl_2$, 5.5 mM dextrose, 10 mM HEPES (pH 7.2). In the LiCl experiments, the pipette solutions contained 145 mM LiCl, 2 mM BAPTA, 1 mM $CaCl_2$, 5 mM HEPES (pH 7.2). TTX (10 μM) was added to the bath solution to reduce nonjunctional currents. All solutions were osmotically balanced at 300 mOsm/kg. In pore-sizing experiments, recording solutions contained 100 mM CsCl, 2 mM TEACl, 2 mM BAPTA, 1 mM $CaCl_2$, 10 mM HEPES (pH 7.2). Nonelectrolytes were added in concentrations sufficient to maintain 300 mOsm/kg; this was 50 mM in the case of the polyethylene glycol series and ~100 mM for mannitol and glycerol. Hydrodynamic radii (Å), taken from Karsilnikov et al. (1995), solution conductivity (mS/cm), and Cl^- activity (mM) of the solutions were, respectively: PEG 900: 9.0, 13.1, and 117; PEG 600: 8.0, 13.6, and 117; PEG 400: 7.0, 14.3, and 115; PEG 300: 5.8, 15, and 115; PEG 200: 4.5, 15, and 111; mannitol: 3.7, 13.4, and not determined (ND); glycerol: 3.1, 13.7, and ND. Pipette resistances were 5–10 MΩ in the bath solution.

Determination of Reversal Potentials in Gap Junctions between Neuro2-A Cells

The contribution of the junctional current (I_j) to the total current, I_t, where $I_t = I_j + I_{nonjunctional}$, measured in the unstepped cell, could be accurately measured only when the cell pair expressed a single channel that underwent a gating transition to $I_j = 0$ or spontaneously uncoupled and recoupled during the application of a set of voltage ramps. Because of this limitation, data are presented for a single cell pair in each experimental condition. Qualitatively similar results (slight anion selectivity and reduced Li^+ permeability) were obtained in cell pairs containing more than one channel, in which the contribution of I_j to I_t was determined at the end of the experiment by killing the ramped cell, which causes junctional conductance to go to zero. These data were not included in the quantitation of permeability due to complications arising from possible differences in the ion selectivities of the fully open and subconductance states and the assumption that $I_{nonjunctional}$ was constant throughout the course of the experiment. P_{Cl}/P_{Cs} was determined using asymmetric (10:1) solutions. The ramped cell contained 147 mM CsCl, 2 mM TEACl, 2 mM BAPTA, 1 mM $CaCl_2$, 5 mM HEPES (pH 7.2) (300 mOsm/kg). The concentration of CsCl in the unramped cell was reduced to 14.7 mM, and osmolarity was adjusted to 300 mOsm/kg by the addition of mannitol. Cells were bathed in the low-salt solution containing 1 mM $CaCl_2$ without BAPTA to reduce the contribution of $I_{nonjunctional}$ current to I_t. Offset potentials in the recording pipettes (5–10 MΩ) were nulled in the bath solution prior to seal formation. In the determination of P_{Li}/P_{Cs}, the ramped cell contained 75 mM LiCl, 2 mM BAPTA, 1 mM $CaCl_2$, 5 mM HEPES (pH 7.2). In the unramped cell, LiCl was replaced with 75 mM CsCl. The bath solution contained 75 mM CsCl, 1 mM $CaCl_2$, 10 μM TTX, and 5 mM HEPES (pH 7.2). All solutions were adjusted to 300 mOsm/kg with mannitol. Prior to whole-cell recording, the potential was set at zero with the pipettes immersed in 3 M KCl to remove liquid-junction potentials. The potential difference between the Cs- and Li-containing pipettes was measured following their transfer to the cell bath solution. The value obtained, 6.9 mV, was close to that predicted by the GHK voltage equation, 7.4 mV, based on the bulk solution mobilities of the ions contained in the recording solutions.

Acknowledgments

We thank Dr. A. Ohnishi for providing DNA samples from the N family, Dr. E. Hertzberg for providing Cx32 antibodies, Jane Zhao and Chris Ginter for technical assistance, and Drs. A. Finkelstein, S. Slatin, and D. Weinstein for helpful discussions. This work was supported by NIH grant GM 46889.

Received May 22, 1997; revised August 26, 1997.

References

Ballesteros, J.A., and Weinstein, H. (1992). Analysis and refinement of criteria for predicting the structure and relative orientations of transmembranal helical domains. Biophys. J. *62*, 107–109.

Barlow, D.J., and Thornton, J.M. (1988). Helix geometry in proteins. J. Mol. Biol. *201*, 601–619.

Bennett, M.V.L. (1994). Connexins in disease. Nature *368*, 18–19.

Bergoffen, J., Scherer, S.S., Wang, M., Oronzi Scott, M., Bone, L.J., Paul, D.L., Chen, K., Lensch, M.W., Chance, P.F., and Fischbeck, K.H. (1993). Connexin mutations in X-linked Charcot-Marie-Tooth disease. Science *262*, 2039–2042.

Bevans, C.G., Kordel, M., Rhee, S., and Harris, A.L. (1997). Connexin channels show differential selectivity among second messengers and uncharged molecules. J. Bol. Chem., in press.

Bezrukov, S.M., and Vodyanoy, I. (1993). Probing alamethicin channels with water-soluble polymers. Effect on conductance of channel states. Biophys. J. *64*, 16–25.

Bone, L.J., Dahl, N., Lensch, M.W., Chance, P.F., Kelley, T., Le Guern, E., Magi, S., Parry, G., Shapiro, H., Wang, S., and Fischbeck, K.H. (1995). New connexin 32 mutations associated with X-linked Charcot-Marie-Tooth disease. Neurology *45*, 1863–1866.

Bruzzone, R., White, T.W., Scherer, S.S., Fischbeck, K.H., and Paul, D.L. (1994a). Null mutations of connexin 32 in patients with X-linked Charcot-Marie-Tooth disease. Neuron *13*, 1253–1260.

Bruzzone, R., White, T.W., and Paul, D.L. (1994b). Expression of chimeric connexins reveals new properties of the formation and gating behavior of gap junction channels. J. Cell Sci. *107*, 955–967.

Bukauskas, F.F., and Weingart, R. (1994). Voltage-dependent gating of single gap junction channels in an insect cell line. Biophys. J. *67*, 613–625.

Chang, M., Werner, R., and Dahl, G. (1996). A role for an inhibitory connexin in testis? Dev. Biol. *175*, 50–56.

Doyle, J.P., and Colman, D.R. (1993). Glial-neuron interactions and the regulation of myelin formation. Curr. Opin. Cell Biol. *5*, 779–785.

Fairweather, N., Bell, C., Cochrane, S., Chelly, J., Wang, S., Mostacciuolo, M.L., Monaco, A.P., and Haites, N.E. (1994). Mutations in the connexin 32 gene in X-linked dominant Charcot-Marie-Tooth disease (CMTX1). Hum. Mol. Genet. *3*, 29–34.

Harris, A.L., Spray, D.C., and Bennett, M.V.L. (1981). Kinetic properties of a voltage-dependent junctional conductance. J. Gen. Physiol. *77*, 95–117.

Harris, A.L., Walter, A., Paul, D., Goodenough, D.A., and Zimmerberg, J. (1992). Ion channels in single bilayers induced by rat connexin 32. Mol. Brain Res. *15*, 269–280.

Hille, B. (1975). Lipid bilayers and biological membranes: dynamic properties. In Membranes—A Series of Advances, Vol. 3, G. Eisenman, ed. (New York: Marcel Dekker), pp. 255–323.

Ionasescu, V., Searby, C., and Ionasescu, R. (1994). Point mutations of the connexin 32 (GJB1) gene in X-linked dominant Charcot-Marie-Tooth neuropathy. Hum. Mol. Genet. *3*, 355–358.

Ionasescu, V., Searby, C., Ionasescu, R., and Meschino, W. (1995). New point mutations and deletions of the connexin 32 gene in X-linked Charcot-Marie-Tooth neuropathy. Neuromusc. Disord. *5*, 297–299.

Ionasescu, V., Ionasescu, R., and Searby, C. (1996). Correlation between connexin 32 gene mutations and clinical phenotype in X-linked dominant Charcot-Marie-Tooth neuropathy. Am. J. Med. Genet. *63*, 486–491.

Kelsell, D.P., Dunlop, J., Stevens, H.P., Lench, N.J., Liang, J.N., Parry, G., Mueller, R.F., and Leigh, I.M. (1997). Connexin 26 mutations in hereditary nonsyndromic sensorineural deafness. Nature *387*, 80–83.

Krasilnikov, O.V., Yuldasheva, L.N., Nogueira, R.A., and Rodrigues, C.G. (1995). The diameter of water pores formed by colicin Ia in planar lipid bilayers. Braz. J. Med. Biol. Res. *28*, 693–698.

Kumar, N.M., and Gilula, N.B. (1986). Cloning and characterization of human and rat liver cDNAs coding for a gap junction protein. J. Cell Biol. *103*, 767–776.

LeBlanc, A.C., Windebank, A.J., and Poduslo, J.F. (1992). P_0 gene expression in Schwann cells is modulated by an increase of cAMP which is dependent on the presence of axons. Mol. Brain Res. *12*, 31–38.

Lemke, G. (1990). Glial growth factors. Semin. Neurosci. *2*, 437–443.

Lemke, G., and Chao, M. (1988). Axons regulate Schwann cell expression of the major myelin and NGF receptor genes. Development *102*, 499–504.

Miller, T., Dahl, G., and Werner, R. (1988). Structure of a gap junction gene: rat connexin-32. Biosci. Rep. *8*, 455–464.

Mirsky, R., and Jessen, K.R. (1996). Schwann cell development, differentiation, and myelination. Curr. Opin. Neurobiol. *6*, 89–96.

Mirsky, R., Winter, J., Abney, E.R., Pruss, R.M., Gavkilovic, J., and Raff, M.C. (1980). Myelin-specific proteins and glycolipids in rat Schwann cells and oligodendrocytes in culture. J. Cell Biol. *84*, 483–494.

Monuki, E.S., Weinmaster, G., Kuhn R., and Lemke G. (1989). SCIP: a glial POU domain gene regulated by cAMP. Neuron *3*, 783–793.

Nicholson, G., and Nash, J. (1993). Intermediate nerve conduction velocities define X-linked Charcot-Marie-Tooth neuropathy families. Neurology *43*, 2558–2564.

Ohnishi, A., Yoshimura, T., Takazawa, A., Hashimoto, T., Yamamoto, T., and Fukushima, Y. (1995). A family of X-linked motor and sensory neuropathy with a new type of connexin 32 mutation. Clin. Neurol. *35*, 843–849.

Omori, Y., Mesnil, M., and Yamasaki, H. (1996). Connexin 32 mutations from X-linked Charcot-Marie-Tooth disease patients: functional defects and dominant negative effects. Mol. Biol. Cell *7*, 907–916.

Orth, U., Fairweather, N., Exler, M.C., Schwinger, E., and Gal, A. (1994). X-linked dominant Charcot-Marie-Tooth neuropathy: valine-38-methionine substitution of connexin 32. Hum. Mol. Genet. *3*, 1699–1700.

Poduslo, J.F., Walikonis, R.S., Domec, M.-C., Berg, C.T., and Holtz-Heppelmann, C.J. (1995). The second messenger, cyclic AMP, is not sufficient for myelin gene induction in the peripheral nervous system. J. Neurochem. *65*, 149–159.

Rabadan-Diehl, C., Dahl, G., and Werner, R. (1994). A connexin-32 mutation associated with Charcot-Marie-Tooth disease does not affect channel formation in oocytes. FEBS Lett. *351*, 90–94.

Renkin, E.M. (1954). Filtration, diffusion, and molecular sieving through porous cellulose membranes. J. Gen. Physiol. *38*, 225–243.

Rozear, M.P., Pericak-Vance, M.A., Fischbeck, K., Stajich, J.M., Gaskell, P.C., Jr., Krendel, D.A., Graham, D.G., Dawson, D.V., and Roses, A.D. (1987). Hereditary motor and sensory neuropathy, X-linked: a half century follow up. Neurology *37*, 1460–1465.

Rubin, J.B., Verselis, V.K., Bennett, M.V.L., and Bargiello, T.A. (1992). Molecular analysis of voltage dependence of heterotypic gap junctions formed by connexins 26 and 32. Biophys. J. *62*, 183–195.

Saez, J.C., Conner, J.A., Spray, D.C., and Bennett, M.V.L. (1989). Hepatocyte gap junctions are permeable to the second messenger, inositol 1,4,5-triphosphate and to calcium ions. Proc. Natl. Acad. Sci. USA *86*, 2708–2712.

Salzer, J.L., Williams, A.K., Glazer, L., and Bunge, R.P. (1980). Studies of Schwann cell proliferation. II. Characterization of the stimulation and specificity of the response to a neurite membrane fraction. J. Cell Biol. *84*, 753–766.

Sankararamakrishnan, R., and Vishveshwara, S. (1992). Geometry of proline-containing alpha-helices in proteins. Int. J. Pept. Protein Res. *39*, 356–363.

Scherer, S.S. (1997). Molecular genetics of demyelination: new wrinkles on an old membrane. Neuron *18*, 13–16.

Scherer, S.S., Deschenes, S.M., Xu, Y., Grinspan, J.B., Fischbeck, K.H., and Paul, D.L. (1995). Connexin 32 is a myelin-related protein in the PNS and CNS. J. Neurosci. *15*, 8281–8294.

Solomon, A.K. (1986). On the equivalent pore radius. J. Membrane Biol. *94*, 227–232.

Suchyna, T.M., Xu, L.X., Gao, F., Fourtner, C.R., and Nicholson, B.J. (1993). Identification of a proline residue as a transduction element involved in voltage gating of gap junction. Nature *365*, 847–849.

Suter, U., Welcher, A.A., and Snipes, G.J. (1993). Progress in the molecular understanding of hereditary peripheral neuropathies reveals new insights into the biology of the peripheral nervous system. Trends Neurosci. *16*, 50–56.

Trexler, E.B., Bennett, M.V.L., Bargiello, T.A., and Verselis, V.K. (1996). Voltage gating and permeation in a gap junction hemichannel. Proc. Natl. Acad. Sci. USA *93*, 5836–5841.

Unger, V.M., Kumar, N.M., Gilula, N.B., and Yeager, M. (1997). Projection structure of a gap junction membrane channel at 7 Å resolution. Nat. Struct. Biol. *4*, 39–43.

Vance, J.M. (1991). Hereditary motor and sensory neuropathies. J. Med. Genet. *28*, 1–5.

Veenstra, R.D. (1996). Size and selectivity of gap junction channels formed from different connexins. J. Bioenerg. Biomembr. *28*, 327–337.

Verselis, V.K., Ginter, C.S., and Bargiello, T.A. (1994). Opposite voltage gating polarities of two closely related connexins. Nature *368*, 348–351.

Vodyanoy, I., and Bezrukov, S.M. (1992). Sizing of an ion pore by access resistance measurements. Biophys. J. *62*, 10–11.

Zhou, X., Pfahnl, A., Werner, R., Hudder, A., Llanes, A., Luebke, A., and Dahl, G. (1997). Identification of a pore lining segment in gap junction hemichannels. Biophys. J. *72*, 1946–1953.

Zorick, T.S., and Lemke, G. (1996). Schwann cell differentiation. Curr. Opin. Cell Biol. *8*, 870–876.